Boise State University
ScholarWorks

CGISS Publications and Presentations

Center for Geophysical Investigation of the Shallow Subsurface (CGISS)

1-1-2007

# Physical Modeling and Analysis of P-Wave Attenuation Anisotropy

Kasper van Wijk
*Boise State University*

GEOPHYSICS, VOL. 72, NO. 1 (JANUARY-FEBRUARY 2007); P. D1–D7, 8 FIGS.
10.1190/1.2374797

# Physical modeling and analysis of P-wave attenuation anisotropy in transversely isotropic media

Yaping Zhu[1], Ilya Tsvankin[2], Pawan Dewangan[3], and Kasper van Wijk[4]

## ABSTRACT

Anisotropic attenuation can provide sensitive attributes for fracture detection and lithology discrimination. This paper analyzes measurements of the P-wave attenuation coefficient in a transversely isotropic sample made of phenolic material. Using the spectral-ratio method, we estimate the group (effective) attenuation coefficient of P-waves transmitted through the sample for a wide range of propagation angles (from 0° to 90°) with the symmetry axis. Correction for the difference between the group and phase angles and for the angular velocity variation help us to obtain the normalized phase attenuation coefficient $\mathcal{A}$ governed by the Thomsen-style attenuation-anisotropy parameters $\epsilon_Q$ and $\delta_Q$. Whereas the symmetry axis of the angle-dependent coefficient $\mathcal{A}$ practically coincides with that of the velocity function, the magnitude of the attenuation anisotropy far exceeds that of the velocity anisotropy. The quality factor $Q$ increases more than tenfold from the symmetry axis (slow direction) to the isotropy plane (fast direction). Inversion of the coefficient $\mathcal{A}$ using the Christoffel equation yields large negative values of the parameters $\epsilon_Q$ and $\delta_Q$. The robustness of our results critically depends on several factors, such as the availability of an accurate anisotropic velocity model and adequacy of the homogeneous concept of wave propagation, as well as the choice of the frequency band. The methodology discussed here can be extended to field measurements of anisotropic attenuation needed for AVO (amplitude-variation-with-offset) analysis, amplitude-preserving migration, and seismic fracture detection.

## INTRODUCTION

Most existing publications on seismic anisotropy are devoted to the influence of angular velocity variation in purely elastic media on the traveltimes and amplitudes of seismic waves. It is likely; however, that anisotropic formations are also characterized by directionally dependent attenuation related to the internal structure of the rock matrix or the presence of aligned fractures or pores (e.g., Mavko and Nur, 1979; MacBeth, 1999; Pointer et al., 2000; Maultzsch et al., 2003).

Various issues related to the analytic treatment of attenuation in anisotropic media were addressed by Borcherdt and Wennerberg (1985), Krebes and Le (1994), Carcione (2001), Červený and Pšenčík (2005), and others. For example, the quality factor $Q$, widely used as a measure of attenuation in isotropic media (e.g., Johnston and Toksöz, 1981), can be replaced by a matrix that describes anisotropic attenuation. Each element $Q_{ij}$ of the quality-factor matrix is defined as the ratio of the real and imaginary parts of the corresponding stiffness coefficient (Carcione, 2001). To facilitate the characterization of anisotropic attenuation, Zhu and Tsvankin (2004, 2006) introduced Thomsen-style attenuation parameters $\epsilon_Q$, $\delta_Q$, and $\gamma_Q$ derived from the $\mathbf{Q}$-matrix for transversely isotropic (TI) media and used the new notation to obtain simple approximations for the angle-dependent attenuation coefficients.

Although experimental measurements of attenuation, both in the field and on rock samples, are relatively rare, they indicate that the magnitude of attenuation anisotropy often exceeds that of velocity anisotropy (e.g., Tao and King, 1990; Arts and Rasolofosaon, 1992; Prasad and Nur, 2003). For example, according to the measurements of Hosten et al. (1987) for an orthorhombic sample made of composite material, the quality factor for P-waves changes from $Q \approx 6$ in the vertical direction to $Q \approx 35$ in the horizontal direction. Hosten et al. (1987) also show that the symmetry of the attenuation coefficient closely follows that of the velocity function.

Manuscript received by the Editor December 14, 2005; revised manuscript received June 25, 2006; published online November 15, 2006.
[1]Formerly Colorado School of Mines, Center for Wave Phenomena, Department of Geophysics; presently Exxon Mobil Upstream Research Company, P. O. Box 2189, Houston, Texas 77252. E-mail: yaping.zhu@exxonmobil.com.
[2]Colorado School of Mines, Center for Wave Phenomena, Department of Geophysics, 1500 Illinois Street, Golden, Colorado 80401. E-mail: ilya@mines.edu.
[3]Formerly Colorado School of Mines, Center for Wave Phenomena, Department of Geophysics; presently Geological Oceanography Division, National Institute of Oceanography, Dona Paula, Goa-403004, India. E-mail: pdewangan@darya.nio.org.
[4]Formerly Colorado School of Mines, Physical Acoustics Laboratory, Department of Geophysics, 1500 Illinois Street, Golden, Colorado 80401; presently Boise State University, Department of Geosciences, 1910 University Drive, Boise, Idaho 83725. E-mail: kasper@dix.mines.edu.
© 2007 Society of Exploration Geophysicists. All rights reserved.

Here, we extend the spectral-ratio method to anisotropic media and apply it to P-wave transmission data acquired in a symmetry plane of a phenolic sample. Fitting the theoretical normalized attenuation coefficient $\mathcal{A}$ to the measurements for a wide range of propagation angles yields estimates of the attenuation-anisotropy parameters $\epsilon_Q$ and $\delta_Q$. Although the experiment was performed for a synthetic material, the results are indicative of the high potential of attenuation-anisotropy analysis for field seismic data.

## THEORETICAL BACKGROUND

### P-wave attenuation in TI media

Propagation of plane P- and SV-waves in TI media with TI attenuation is described by the Christoffel equation (e.g., Carcione, 2001):

$$(\tilde{c}_{11}\tilde{k}_1^2 + \tilde{c}_{55}\tilde{k}_3^2 - \rho\omega^2)(\tilde{c}_{55}\tilde{k}_1^2 + \tilde{c}_{33}\tilde{k}_3^2 - \rho\omega^2) - [(\tilde{c}_{13} + \tilde{c}_{55})\tilde{k}_1\tilde{k}_3]^2 = 0, \quad (1)$$

where $\rho$ is the density, $\omega$ is the angular frequency, $\tilde{c}_{ij} = c_{ij} + ic_{ij}^I$ are the complex stiffness coefficients (the symbol "$\sim$" above a letter denotes a complex variable), and $\tilde{\mathbf{k}} = \mathbf{k} - i\mathbf{k}^I$ is the complex wave vector. Generally, the vectors $\mathbf{k}$ and $\mathbf{k}^I$ (the imaginary part $\mathbf{k}^I$ is sometimes called the attenuation vector) have different orientations, which means that phase (slowness) direction does not coincide with the direction of maximum attenuation. In that case, wave propagation is often called inhomogeneous, and the angle between $\mathbf{k}$ and $\mathbf{k}^I$ is called the inhomogeneity angle. Whereas the inhomogeneity angle represents a free parameter in plane-wave propagation, it is usually small for wavefields excited by point sources in weakly attenuative, weakly anisotropic media (for more details, see Zhu and Tsvankin, 2006). Hereafter, we assume that wave propagation is homogeneous and $\tilde{\mathbf{k}} = \mathbf{n}(k - ik^I)$, where $\mathbf{n}$ is the unit slowness vector.

As discussed in Carcione (2001) and Zhu and Tsvankin (2006), the Christoffel equation 1 yields the (real-valued) phase velocity $v = \omega/k$ and the normalized attenuation coefficient $\mathcal{A} = k^I/k$. The coefficient $\mathcal{A}$, which determines the rate of amplitude decay per wavelength, is expressed through the quality-factor matrix ($Q_{ij} \equiv c_{ij}/c_{ij}^I$) and the real parts $c_{ij}$ of the stiffnesses $\tilde{c}_{ij}$. Even for the relatively simple medium in which both $c_{ij}$ and $c_{ij}^I$ have TI (hexagonal) symmetry, the exact attenuation coefficients of P- and SV-waves have a rather complicated form.

To facilitate analytic description of TI attenuation, Zhu and Tsvankin (2004, 2006) suggested a notation based on the same principle as the commonly used Thomsen (1986) parameters for velocity anisotropy. For P- and SV-waves, the set of Thomsen-style attenuation-anisotropy parameters includes $\mathcal{A}_{P0}$, $\mathcal{A}_{S0}$, $\epsilon_Q$, and $\delta_Q$ (see Appendix A). The parameters $\mathcal{A}_{P0}$ and $\mathcal{A}_{S0}$ are the P- and S-wave attenuation coefficients (respectively) in the symmetry direction, while $\epsilon_Q$ and $\delta_Q$ control the angle variation of the attenuation coefficients between the symmetry axis and the isotropy plane. In the limit of small attenuation and weak anisotropy (for both velocity and attenuation), the P-wave attenuation coefficient can be significantly simplified by linearizing the solution of the Christoffel equation 1 in the anisotropy parameters (Zhu and Tsvankin, 2006):

$$\mathcal{A} = \mathcal{A}_{P0}(1 + \delta_Q \sin^2\theta\cos^2\theta + \epsilon_Q \sin^4\theta), \quad (2)$$

where $\theta$ is the phase angle with the symmetry axis.

Equation 2 has exactly the same form as Thomsen's (1986) weak-anisotropy approximation for the P-wave phase velocity. The parameter $\delta_Q$ is responsible for the attenuation coefficient in near-vertical directions, while $\epsilon_Q$ controls $\mathcal{A}$ near the horizontal plane. The definition of the parameter $\delta_Q$; however, is more complicated than that of Thomsen's parameter $\delta$ and reflects the coupling between the anisotropy of attenuation and velocity. If both $\epsilon_Q$ and $\delta_Q$ go to zero, the approximate coefficient $\mathcal{A}$ becomes isotropic (i.e., independent of angle). Note that the exact attenuation coefficient $\mathcal{A}$ is somewhat dependent on the velocity parameters $\epsilon$ and $\delta$ in addition to $\epsilon_Q$ and $\delta_Q$ (Zhu and Tsvankin, 2006).

### Spectral-ratio method for anisotropic attenuation

The spectral-ratio method is often used to estimate the attenuation coefficient in both physical modeling and field surveys. For laboratory experiments, application of this method typically involves amplitude measurements made under identical conditions for the sample of interest and for a purely elastic (nonattenuative) reference sample.

The frequency-domain displacement of the direct wave recorded for the reference nonattenuative homogeneous sample [the superscript (0)] can be written as

$$U^{(0)}(\omega) = S(\omega)\, G^{(0)}(\mathbf{x}^{(0)})\, e^{i\omega(t-|\mathbf{x}^{(0)}|/V_G^{(0)})}, \quad (3)$$

where $\mathbf{x}$ is the vector connecting the source and receiver, $V_G$ is the group (ray) velocity in the direction $\mathbf{x}$, $S(\omega)$ is the spectrum of the source pulse, and the factor $G(\mathbf{x})$ incorporates the radiation pattern of the source and the geometrical spreading along the raypath. Similarly, the frequency-domain displacement for the attenuative sample [the superscript (1)] has the form

$$U^{(1)}(\omega) = S(\omega)\, G^{(1)}(\mathbf{x}^{(1)})\, e^{-k_G^I|\mathbf{x}^{(1)}|}\, e^{i\omega(t-|\mathbf{x}^{(1)}|/V_G^{(1)})}; \quad (4)$$

$k_G^I$ is the amplitude decay factor (attenuation coefficient) in the group (ray) direction.

The logarithm of the amplitude ratio can be found from equations 3 and 4 as

$$\ln\left|\frac{U^{(1)}}{U^{(0)}}\right| = \ln\left(\frac{G^{(1)}}{G^{(0)}}\right) - k_G^I|\mathbf{x}^{(1)}|. \quad (5)$$

The frequency dependence of the term $G^{(1)}/G^{(0)}$ is usually considered to be negligible in the frequency band of interest. Then the slope of $\ln|U^{(1)}/U^{(0)}|$ expressed as a function of the frequency $\omega$ yields the local value of the inverse $Q$-factor in the source-receiver direction. If this slope changes with $\omega$, then the assumption of frequency-independent $Q$ is not valid.

In isotropic media with isotropic (angle-invariant) attenuation, the group attenuation coefficient $k_G^I$ measured along the raypath coincides with the phase (plane-wave) attenuation coefficient $k^I$. For anisotropic media with anisotropic attenuation; however, these two coefficients generally differ. If wave propagation is homogeneous (i.e., the inhomogeneity angle is negligible), the group and phase attenuation coefficients are related by the equation $k_G^I = k^I \cos\hat{\psi}$, where $\hat{\psi}$ is the angle between the group- and phase-velocity vectors (Zhu and Tsvankin, 2004).

Then the normalized phase attenuation coefficient introduced above is given by

$$\mathcal{A} = \frac{k^I}{k} = \frac{k^I}{\omega} V = \frac{k_G^I}{\omega \cos \hat{\psi}} V, \tag{6}$$

where $V$ is the phase velocity that corresponds to the source-receiver (group) direction (i.e., $V$ is the velocity of the plane wave tangential to the wavefront at the receiver location). Therefore, the coefficient $\mathcal{A}$ can be found as the measured slope of the group attenuation coefficient $k_G^I(\omega)$ scaled by the ratio $V/\cos \hat{\psi}$.

Here, we employ the following procedure of inverting P-wave attenuation measurements for the attenuation-anisotropy parameters. First, the slope of the logarithmic spectral ratio in equation 5 expressed as a function of $\omega$ is used to estimate $k_G^I/\omega$. Second, using the velocity parameters of the sample (assumed to be known), we compute the phase velocity $V$ and angle $\hat{\psi}$ and substitute them into equation 6 to find the coefficient $\mathcal{A}$. Third, the measurements of $\mathcal{A}$ for a wide range of phase angles are inverted for the attenuation-anisotropy parameters $\epsilon_Q$ and $\delta_Q$. Approximate values of $\epsilon_Q$ and $\delta_Q$ can be found in a straightforward way from the linearized equation 2. More accurate results; however, are obtained by nonlinear inversion based on the exact Christoffel equation 1.

Because of the dependence of the exact coefficient $\mathcal{A}$ on the velocity parameters (Zhu and Tsvankin, 2006) and the contribution of the velocity anisotropy to equation 6, estimation of $\epsilon_Q$ and $\delta_Q$ requires knowledge of the anisotropic velocity field. Since the influence of attenuation on velocity typically is a second-order factor, anisotropic velocity analysis can be performed prior to attenuation measurements. In the inversion below we use the results of Dewangan (2004) and Dewangan et al. (2006), who estimated the velocity-anisotropy parameters of our sample by inverting reflection traveltimes of PP- and PS-waves.

## EXPERIMENTAL SETUP AND DATA PROCESSING

Our goals were to measure the directional dependence of the P-wave attenuation coefficient in a composite sample and invert these measurements for the attenuation-anisotropy parameters $\epsilon_Q$ and $\delta_Q$. We used XX-paper-based phenolic material composed of thin layers of paper bonded with phenolic resin. This fine layering produces an effective anisotropic medium on the scale of the predominant wavelength. The sample was prepared by Dewangan (2004; Figure 1), who pasted phenolic blocks together at an angle, which resulted in a transversely isotropic model with the symmetry axis tilted from the vertical by 70° (TTI medium). Laser-Doppler measurements of the vertical component of the wavefield were made by van Wijk in the Physical Acoustic Laboratory at Colorado School of Mines.

Dewangan et al. (2006) show that the TTI model adequately explains the kinematics of multicomponent (P, S, and PS) data in the vertical measurement plane that contains the symmetry axis (called the symmetry-axis plane). Although phenolic materials are generally known to be orthorhombic (e.g., Grechka et al., 1999), body-wave velocities and polarizations in the symmetry planes of orthorhombic media can be described by the corresponding TI equations (Tsvankin, 1997, 2005).

The original purpose of acquiring the transmission data used here (Figures 1 and 2a) was to verify the accuracy of the parameter-estimation results obtained by Dewangan et al. (2006). The P-wave source (a flat-faced, cylindrical, piezoelectric-contact transducer) was fixed at the bottom of the model and the wavefield was recorded by a laser vibrometer at an interval of 2 mm. The spread of the receiver locations was wide enough to cover a full range of propagation angles (from 0° to 90°) with respect to the (tilted) symmetry axis.

To perform attenuation analysis, we separated the first (direct) arrival by applying a Gaussian window to the raw data. The amplitude spectrum of the windowed first arrival obtained by filtering out the low ($f < 5$ kHz) and high ($f > 750$ kHz) frequencies is shown in Figure 2b. An aluminum block with negligibly small attenuation served as the reference model. The reference trace was acquired by a receiver located directly opposite the source (Figure 3).

For each receiver position at the surface of the phenolic sample, we divided the spectrum of the windowed recorded trace by that of the reference trace to compute the spectral ratio (equation 5). Records with a low signal-to-noise ratio were excluded from the analysis. Note that Figures 2b and 3 reveal gaps in the frequency spectrum (around 170 and 200 kHz, respectively), which are likely related to the mechanical properties of the piezoelectric source. To estimate the group-attenuation coefficient $k_G^I$ from equation 5, we chose a frequency band (60–110 kHz) away from the spectral gaps. According to the spectral-ratio method described above, the relevant elements $Q_{ij}$ in that frequency band are assumed to be constant.

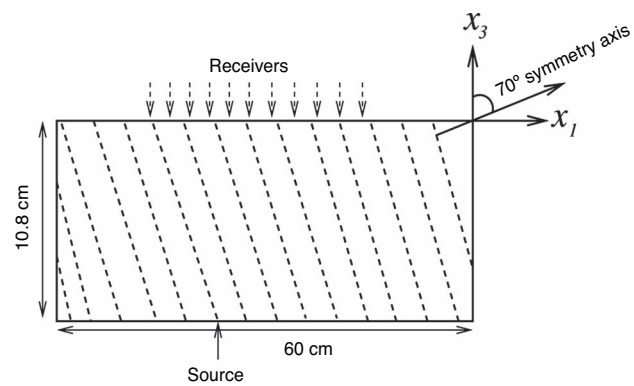


Figure 1. Physical model of a TI layer with the symmetry axis tilted at 70° (from Dewangan et al., 2006). The transmitted wavefield is excited by an ultrasonic contact transducer at the bottom of the model and recorded by a laser vibrometer.

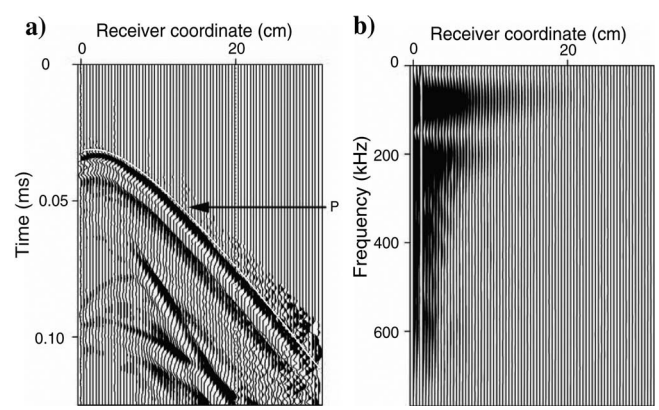


Figure 2. (a) Raw transmitted wavefield excited by a P-wave transducer and (b) the amplitude spectrum of the windowed first arrival. The solid curve is the P-wave traveltime modeled by Dewangan et al. (2006) using the inverted parameters from Figure 4. The time sampling interval is $2\mu$s and the width of the Gaussian window is 40 samples.

## EVALUATION OF ATTENUATION ANISOTROPY

The parameters of the TTI velocity model needed to process the attenuation measurements were obtained by Dewangan et al. (2006) from reflection PP and PS data (Figure 4). Tilted transverse isotropy is described by the P- and S-wave velocities in the symmetry direction ($V_{P0}$ and $V_{S0}$, respectively), Thomsen anisotropy parameters $\epsilon$ and $\delta$ defined with respect to the symmetry axis, the angle $\nu$ between the symmetry axis and the vertical, and the thickness $z$ of the sample. The known values of $\nu = 70°$ and $z = 10.8$ cm were accurately estimated from the reflection data, which confirms the robustness of the velocity-inversion algorithm.

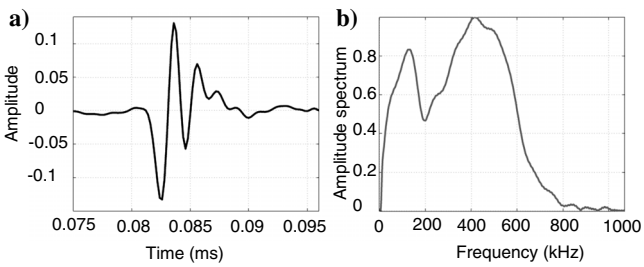


Figure 3. (a) Reference trace for vertical propagation through an aluminum block and (b) its amplitude spectrum.

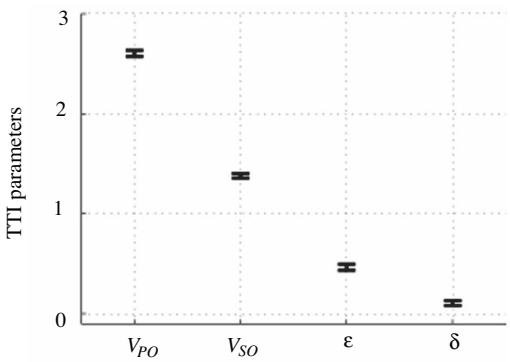


Figure 4. Parameters of the TTI model estimated from reflection traveltimes of PP- and PS-waves in the symmetry-axis plane (after Dewangan et al., 2006). The mean values are $V_{P0} = 2.6$ km/s, $V_{S0} = 1.38$ km/s, $\epsilon = 0.46$, and $\delta = 0.11$. The error bars mark the standard deviations in each parameter obtained by applying the inversion algorithm to 200 realizations of input reflection traveltimes contaminated by Gaussian noise. The standard deviation of the noise was equal to one-eighth of the dominant period of the reflection arrivals.

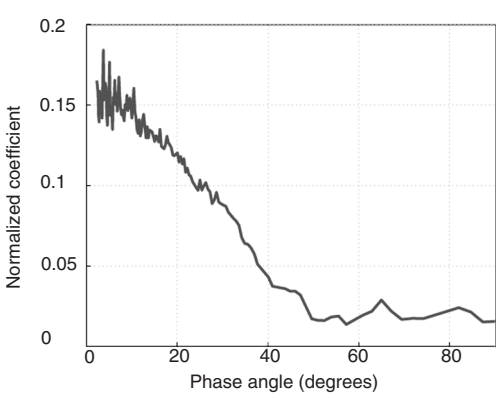


Figure 5. Normalized attenuation coefficient $\mathcal{A}$ as a function of the phase angle $\theta$ with the symmetry axis.

### Estimation of the attenuation-anisotropy parameters

Using the computed slope of the function $k_G^I(\omega)$ for each receiver location and the velocity parameters of the sample (Figure 4), we found the normalized phase-attenuation coefficient $\mathcal{A}$ from equation 6. Note that the difference between the group and phase-attenuation coefficients for our model does not exceed 6%. The coefficient $\mathcal{A}$ exhibits an extremely pronounced variation between the slow (0°) and fast (90°) directions (Figure 5). The largest attenuation is observed along the symmetry axis ($\theta = 0°$), where the P-wave phase velocity reaches its minimum value. Since the symmetry direction is orthogonal to the multiple thin layers bonded together to form the model, the rapid increase in attenuation toward $\theta = 0°$ could be expected.

The polar plot of the attenuation coefficient (Figure 6) indicates that the symmetry axis of the function $\mathcal{A}(\theta)$ is close to that for the velocity measurements. Although we did not acquire data for angles over 90° to reconstruct a more complete angle variation of $\mathcal{A}$, the direction orthogonal to the layering should indeed represent the symmetry axis for all physical properties of the model. To quantify the attenuation anisotropy, we used the Christoffel equation 1 to estimate the best-fit parameters $\mathcal{A}_{P0} = 0.16$ ($Q_{33} = 3.2$), $\epsilon_Q = -0.92$, and $\delta_Q = -1.84$. The small-attenuation, weak-anisotropy approximation (equation 2) yields similar values ($\mathcal{A}_{P0} = 0.16$, $\epsilon_Q = -0.86$, and $\delta_Q = -1.91$) despite the large magnitude of the angle variation of $\mathcal{A}$ (Figure 6).

Though it is predictable that the largest attenuation coefficient for this model should be observed at the velocity minimum, the extremely low value of $Q_{33} = 3.2$ is somewhat surprising. It should be mentioned; however, that the estimates of the attenuation coefficient near the symmetry axis may have been distorted by the relatively low reliability of amplitude measurements at long offsets corresponding to small angles $\theta$ (Figure 1). Problems in applying our methodology for large source-receiver distances may be related to such factors as frequency-dependent geometric spreading and increased influence of heterogeneity.

An essential assumption behind the estimates of the attenuation-anisotropy parameters is that the inhomogeneity angle is negligibly small. Although the modeled attenuation coefficient provides a good fit to the measured curve, it is not clear how significant the inhomogeneity angle for this model may be and how it can influence the parameter-estimation results. Moreover, the coupling of the source with the reference aluminum block differs from that of the phenolic sample, which can influence the source spectra and cause errors in the attenuation estimation.

### Uncertainty analysis

It is important to evaluate the uncertainty of the attenuation measurements caused by possible errors in the velocity-anisotropy parameters. Using the standard deviations in the parameters $V_{P0}$, $\epsilon$, $\delta$, and $\nu$ provided by Dewangan et al. (2006), we repeated our inversion procedure for 50 realizations of the input TTI velocity model (Figure 7). Although the variation of the estimated attenuation coefficients in some directions is substantial, the mean values of the attenuation-anisotropy parameters obtained from the best-fit curve $\mathcal{A}(\theta)$ are close to those listed above. The standard deviations are 2%

for $\mathcal{A}_{P0}$, 0.01 for $\epsilon_Q$, and 0.06 for $\delta_Q$, indicating that the influence of moderate errors in the velocity field on our results is not significant.

Another potential source of uncertainty in the attenuation-anisotropy measurements is the choice of the frequency band used in the spectral-ratio method. Figure 8 shows the distribution of 50 realizations of the attenuation-anisotropy parameters obtained for variable upper and lower bounds of the frequency band. The means of the estimated parameters are $\mathcal{A}_{P0} = 0.16$, $\epsilon_Q = -0.90$, and $\delta_Q = -1.94$, with standard deviations of 3% for $\mathcal{A}_{P0}$, 0.06 for $\epsilon_Q$, and 0.15 for $\delta_Q$. Therefore, the sensitivity of the attenuation-anisotropy parameters to moderate variations in the bounds of the frequency band is not negligible.

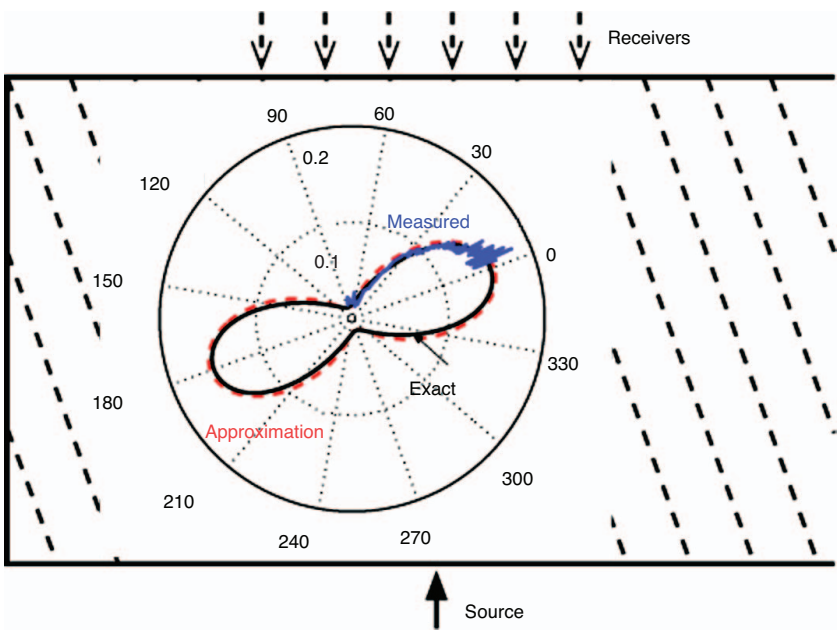


Figure 6. Polar plot of the attenuation coefficient against the background of our physical model. The estimated function $\mathcal{A}(\theta)$ from Figure 5 (blue curve) was used to find the best-fit attenuation coefficient from the Christoffel equation 1 (black) and approximate equation 2 (dashed). The numbers on the perimeter indicate the phase angle with the symmetry axis.

In accordance with the spectral-ratio method, we assume the quality-factor components $Q_{ij}$ to be frequency-independent within the frequency band used in the analysis. However, observed variations of the slope of the coefficient $k_G^I$ in the frequency domain indicate that $Q_{ij}$ and the attenuation-anisotropy parameters may vary with frequency.

## DISCUSSION

While the large difference between the attenuation coefficients in the two principal directions is unquestionable, the accuracy of our measurements strongly depends on several assumptions. First, the radiation pattern of the source and the geometrical spreading are taken to be frequency independent in the frequency band used in the spectral-ratio method. Because of the possible influence of heterogeneity, it is desirable to test the validity of this assumption, particularly for relatively large source-receiver offsets. For example, the experiment can be redesigned by making measurements on two different-size samples of the same phenolic material. Then it would be possible to compute the spectral ratios for arrivals propagating in the same direction and recorded at different distances from the source. In this case, the potential frequency dependence of the radiation pattern would be removed from the attenuation measurement along with the spectrum of the source pulse and no reference trace would be required.

Second, our analytic solutions for the attenuation coefficient are based on the common assumption of homogeneous wave propagation (i.e., the inhomogeneity angle is assumed to be negligible). For strongly attenuative models with pronounced attenuation anisotropy, this assumption may cause errors in the interpretation of attenuation measurements. In particular, if the model is layered, the inhomogeneity angle is governed by the boundary conditions and can be significant even for moderate values of the attenua-

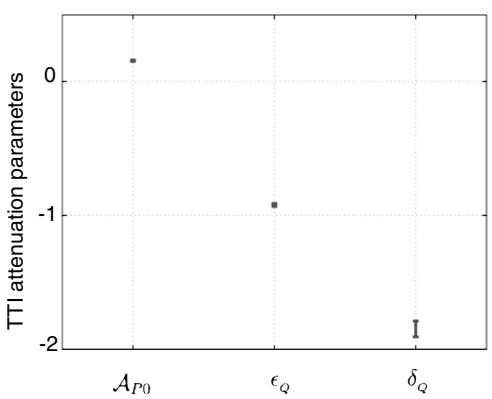


Figure 7. Influence of errors in the velocity model on the attenuation parameters. The error bars mark the standard deviation in each inverted parameter obtained by applying our algorithm with 50 realizations of the input TTI velocity model. The standard deviations in the TTI parameters are taken from Dewangan et al. (2006).

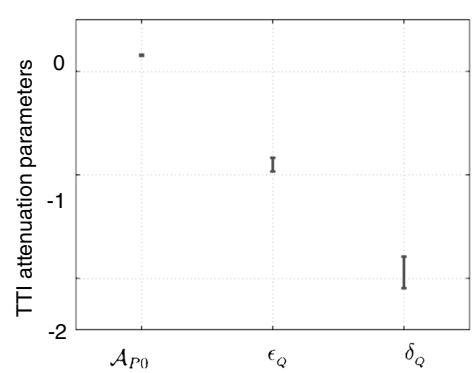


Figure 8. Influence of the frequency band used in the spectral-ratio method on the attenuation parameters. The error bars mark the standard deviation in each parameter obtained by applying our algorithm with 50 realizations of the upper and lower bounds of the frequency band. The upper bound was changed randomly between 88 and 132 kHz, and the lower bound between 44 and 66 kHz.

tion coefficients. Hence, future work should include evaluation of the magnitude of the inhomogeneity angle and of its influence on the estimation of the attenuation-anisotropy parameters.

Third, our data-processing sequence did not include compensation for a possible attenuation-related frequency dependence of the reflection/transmission coefficients along the raypath. Moreover, choice of the frequency band can change the results of attenuation analysis.

Finally, since this work was restricted to P-waves, we did not evaluate the strength of the shear-wave attenuation anisotropy and estimate the full set of Thomsen-style anisotropy parameters. A more complete characterization of attenuation anisotropy requires combining compressional data with either shear or mode-converted waves.

## CONCLUSIONS

Since case studies involving attenuation measurements are scarce, physical modeling can provide valuable insights into the behavior of attenuation coefficients and the performance of seismic algorithms for attenuation analysis. Here, we extended the spectral-ratio method to anisotropic materials and applied it to P-waves transmitted through a transversely isotropic sample for a wide range of propagation angles. After estimating the group (effective) attenuation along the raypath, we computed the corresponding phase (plane-wave) attenuation coefficient $\mathcal{A}$ using the known TI velocity model. The difference between the phase and group attenuation, caused by the influence of velocity anisotropy, has to be accounted for in the inversion for the attenuation-anisotropy parameters.

The angle-varying coefficient $\mathcal{A}$ was used to estimate the Thomsen-style attenuation parameters $\mathcal{A}_{P0}$, $\epsilon_Q$, and $\delta_Q$. The large absolute values of both $\epsilon_Q = -0.92$ and $\delta_Q = -1.84$ reflect the extremely high magnitude of the attenuation anisotropy, with the $Q$-factor increasing from 3.2 in the slow (symmetry-axis) direction to almost 40 in the fast (isotropy-plane) direction.

Our results corroborate the conclusions of some previous experimental studies that attenuation is often more sensitive to anisotropy than phase velocity or reflection coefficient. In particular, we believe that the attenuation-anisotropy parameters will become valuable seismic attributes in characterization of fractured reservoirs.

## ACKNOWLEDGMENTS

We are grateful to Mike Batzle of the Center for Rock Abuse at Colorado School of Mines (CSM) for his help in data acquisition and to Ivan Vasconcelos and Manika Prasad (both of CSM) for useful discussions. We thank the editors and reviewers of GEOPHYSICS for their constructive comments. Support for this work was provided by the Consortium Project on Seismic Inverse Methods for Complex Structures at the CSM Center for Wave Phenomena. K. van Wijk is supported by the National Science Foundation (EAR-0337379) and the Army Research Office (DAAD19-03-1-0292).

## APPENDIX A

## THOMSEN-STYLE PARAMETERS FOR ATTENUATIVE TI MEDIA

The attenuation coefficients in TI media with TI attenuation can be conveniently described using the Thomsen-style notation of Zhu and Tsvankin (2004, 2006). Instead of the five independent components $Q_{ij}$ of the quality-factor matrix, they defined two isotropic reference quantities ($\mathcal{A}_{P0}$ and $\mathcal{A}_{S0}$) and three dimensionless parameters ($\epsilon_Q$, $\delta_Q$, and $\gamma_Q$) responsible for the attenuation anisotropy.

$\mathcal{A}_{P0}$ and $\mathcal{A}_{S0}$ represent the P- and S-wave attenuation coefficients (respectively) in the symmetry direction:

$$\mathcal{A}_{P0} \equiv \frac{1}{2Q_{33}}, \tag{A-1}$$

$$\mathcal{A}_{S0} \equiv \frac{1}{2Q_{55}}. \tag{A-2}$$

Note that equations A-1 and A-2 are accurate to the second order in $1/Q_{ii}$.

The parameter $\epsilon_Q$ denotes the fractional difference between the P-wave attenuation coefficients in the isotropy plane and along the symmetry axis:

$$\epsilon_Q \equiv \frac{1/Q_{11} - 1/Q_{33}}{1/Q_{33}} = \frac{Q_{33} - Q_{11}}{Q_{11}}. \tag{A-3}$$

Another attenuation-anisotropy parameter, $\delta_Q$, is expressed through the curvature of the P-wave attenuation coefficient $\mathcal{A}$ in the symmetry direction. Therefore, $\delta_Q$ governs the variation of $\mathcal{A}$ with the phase angle $\theta$ near the symmetry axis:

$$\delta_Q \equiv \frac{1}{2\mathcal{A}_{P0}} \left.\frac{d^2\mathcal{A}(\theta)}{d\theta^2}\right|_{\theta=0}$$

$$= \frac{\dfrac{Q_{33} - Q_{55}}{Q_{55}} c_{55} \dfrac{(c_{13} + c_{33})^2}{(c_{33} - c_{55})} + 2\dfrac{Q_{33} - Q_{13}}{Q_{13}} c_{13}(c_{13} + c_{55})}{c_{33}(c_{33} - c_{55})} \tag{A-4}$$

$$\approx 4\frac{Q_{33} - Q_{55}}{Q_{55}} g + 2\frac{Q_{33} - Q_{13}}{Q_{13}}(1 + 2\delta - 2g), \tag{A-5}$$

where $g \equiv V_{S0}^2/V_{P0}^2$ is the squared vertical-velocity ratio. Equation A-5 is a linearized approximation valid for $|\delta| \ll 1$ and $g \ll 1$. The dependence of $\delta_Q$ on the velocity parameter $\delta$ is indicative of the coupling between the attenuation coefficient and velocity anisotropy. The third anisotropic parameter, $\gamma_Q$ (not used in this paper), is responsible for the attenuation anisotropy of SH-waves.

The approximate P-wave attenuation coefficient in terms of the parameters $\mathcal{A}_{P0}$, $\epsilon_Q$, and $\delta_Q$ is given in the main text (equation 2).

## REFERENCES

Arts, R. J., and P. N. J. Rasolofosaon, 1992, Approximation of velocity and attenuation in general anisotropic rocks: 62nd Annual International Meeting, SEG, Expanded Abstracts, 640–643.

Borcherdt, R. D., and L. Wennerberg, 1985, General P, type-I S, and type-II S waves in anelastic solids; Inhomogeneous wave fields in low-loss solids: Bulletin of the Seismological Society of America, **75**, 1729–1763.

Carcione, J. M., 2001, Wave fields in real media: Wave propagation in anisotropic, anelastic, and porous media: Pergamon Press, Inc.

Červený, V., and I. Pšenčík, 2005, Plane waves in viscoelastic anisotropic media, part I: Theory: Geophysical Journal International, **161**, 197–212.

Dewangan, P., 2004, Processing and inversion of mode-converted waves using the PP + PS = SS method: Ph.D. thesis, Colorado School of Mines.

Dewangan, P., I. Tsvankin, M. Batzle, K. van Wijk, and M. Haney, 2006, PS-wave moveout inversion for tilted TI media: A physical-modeling study: Geophysics, **71**, D135–D143.

Grechka, V., S. Theophanis, and I. Tsvankin, 1999, Joint inversion of P- and PS-waves in orthorhombic media: Theory and a physical modeling study: Geophysics, **64**, 146–161.

Hosten, B., M. Deschamps, and B. R. Tittmann, 1987, Inhomogeneous wave generation and propagation in lossy anisotropic solids: Application to the characterization of viscoelastic composite materials: Journal of the Acoustical Society of America, **82**, 1763–1770.
Johnston, D. H., and M. N. Toksöz, 1981, Definitions and terminology, *in* D. H. Johnston and M. N. Toksöz, eds., Seismic wave attenuation: Geophysics Reprint Series no. 2: SEG, 1–5.
Krebes, E. S., and L. H. T. Le, 1994, Inhomogeneous plane waves and cylindrical waves in anisotropic anelastic media: Journal of Geophysical Research, **99**, 23,899–23,919.
MacBeth, C., 1999, Azimuthal variation in P-wave signatures due to fluid flow: Geophysics, **64**, 1181–1192.
Maultzsch, S., E. Liu, and M. Chapman, 2003, Modeling attenuation anisotropy and its interpretation in terms of fracture properties: 73rd Annual International Meeting, SEG, Expanded Abstracts, 109–112.
Mavko, G. M., and A. Nur, 1979, Wave attenuation in partially saturated rocks: Geophysics, **44**, 161–178.
Pointer, T., E. Liu, and J. A. Hudson, 2000, Seismic wave propagation in cracked porous media: Geophysical Journal International, **142**, 199–231.
Prasad, M., and A. Nur, 2003, Velocity and attenuation anisotropy in reservoir rocks: 73rd Annual International Meeting, SEG, Expanded Abstracts, 1652–1655.
Tao, G., and M. S. King, 1990, Shear-wave velocity and Q anisotropy in rocks: A laboratory study: International Journal of Rock Mechanics and Mining Sciences & Geomechanics Abstracts, **27**, 353–361.
Thomsen, L., 1986, Weak elastic anisotropy: Geophysics, **51**, 1954–1966.
Tsvankin, I., 1997, Anisotropic parameters and P-wave velocity for orthorhombic media: Geophysics, **62**, 1292–1309.
———, 2005, Seismic signatures and analysis of reflection data in anisotropic media, 2nd ed.: Elsevier Science Pub. Co., Inc.
Zhu, Y., and I. Tsvankin, 2004, Plane-wave propagation and radiation patterns in attenuative TI media: 74th Annual Internatational Meeting SEG, Expanded Abstracts, 139–142.
———, 2006, Plane-wave propagation in attenuative transversely isotropic media: Geophysics, **71**, T17–T30.